THE INFLUENCE OF CHEMISTRY INHOMOGENEITY ON MICROSTRUCTURE DEVELOPMENT AND RESIDUAL STRESS

J. NI*, J. VANDE VOORDE**, J. ANTONISSEN** and M. A. WAHAB*

*Laboratory Soete, Faculty of Engineering and Architecture, Ghent University, 9052, Zwijnaarde, Belgium
**Research Centre for the Application of Steel (OCAS), 9060, Zelzate, Belgium

DOI 10.3217/978-3-85125-615-4-08

ABSTRACT

The chemistry distribution is of importance in the welding process. By varying the chemical composition, the evolution of microstructure and the residual stress change correspondingly. To examine the effect of chemistry, a three-dimensional metallo-thermo-mechanical model is created. The model is established according to a bead-on-plate welding experiment. Samples of S700 steel are manufactured by gas metal arc welding (GMAW). In total, three welds with three heat inputs were conducted so that different chemistries are obtained. The final weld geometry and the uniform chemistry in the fusion zone (FZ) are predicted by the software SimWeld. The parameters in the double ellipsoidal heat source are also calibrated by SimWeld. An inhomogeneous chemistry field is created using the data predicted by SimWeld and the chemical composition of base material (BM), and is further imported to the coupled model by writing user subroutine in ABAQUS. The metallurgical algorithm is implemented in the same way for calculating the phase volume fraction using both the homogeneously and the inhomogeneously distributed chemistry fields. After the temperature and microstructure are determined, the mechanical analysis is conducted using linearly interpolated material properties. Finally, the results of microstructure distribution and the residual stress predicted for homogeneous and inhomogeneous field are compared to clarify the influence of chemical composition.

Keywords: Chemistry Inhomogeneity, Residual stress, Phase transformation

INTRODUCTION

The filler wire and the base material are mixed during the welding process, leading to an area whose chemical composition is neither that of the filler nor that of the base. This variation in the chemical composition will definitely cause a change in microstructure evolution. However, due to the complexity of the welding process, the chemical composition in FZ is hard to predict. Buki [1] developed an algorithm to calculate the composition, and applied it as a universal procedure to design new electrodes. However, this method is not widely adopted. An alternative way to predict the chemistry in FZ is provided by the commercial software SimWeld. This approach is adopted in this research work.

When conducting the metallurgical simulation, several authors [2-4] simply treated the chemistry in FZ the same as in BM, which is obviously not reasonable. An improvement was done by using two chemical compositions, the one of filler for FZ, and the other of BM for the rest of the welded structures [5]. Both compositions are homogeneously distributed in corresponding regions. However, this assumption may not hold since the chemical compositions of BM and filler mix in the FZ, leading to an area with chemistry of neither BM nor filler. To consider this effect, SimWeld is used to estimate the chemical composition in FZ for constructing the complete chemistry field. This field is then imported to the metallurgical algorithm of Bhadeshia et al. [6-9] by assigning the chemical composition to each node of finite element (FE) model.

In this work, the arc welding was conducted with three levels of input power. Therefore, the wire filler and the base material contribute in different ratios to the FZ. As a result, different chemistry fields are achieved. The chemical composition in FZ as well as the final geometry of the weldments are predicted by SimWeld. Those data are imported into ABAQUS to create coupled models. Finally, the phase volume fractions and the residual stress distributions predicted using only the BM and the non-uniform chemistry fields are compared to demonstrate the influence of chemistry inhomogeneity.

TRANSFORMATION KINETICS

The kinetic functions of the austenite decomposition are briefly introduced in this section. As the temperature decreases, austenite transforms to allotriomorphic ferrite, Widmannstätten ferrite, pearlite, bainite and martensite, which are written in symbols of γ, α, α_w, α_p, α_b and α', respectively.

γ continues to decompose until the space of the austenite grain is fully filled. The space is evaluated by the grain boundary area O_B of austenite as [10]:

$$O_B = \frac{2}{\overline{L}} \tag{1}$$

where $\overline{L}$ is the mean linear intercept for an equiaxial grain.

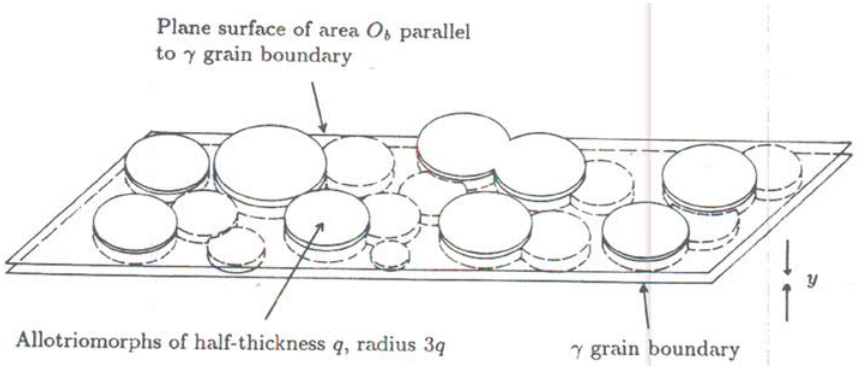

Fig. 1 Representative plot of α grain growth [11]

α is assumed to grow layer by layer as shown in Figure 1, in which the growth of it is modelled as expansion and thickening of discs. Those discs are assumed to be able to grow on both sides of γ grain boundaries with the half-thickness q_α as [6]:

$$q_\alpha = \upsilon_\alpha (t-\tau)^{1/2} \tag{2}$$

where υ_α is the parabolic thickening rate, and τ is the incubation time. The change rate of the area that intersects with the plane at a distance of y away from grain boundary at time $t=m\Delta t$ is given as [6]:

$$A_{\alpha,k,y} = \begin{cases} \pi\eta_\alpha^{\,2}\upsilon_\alpha^{\,2} & q_{\alpha,m\Delta t} > y \\ \pi\eta_\alpha^{\,2} q_{\alpha,m\Delta t}^{\,2} / \Delta t & q_{\alpha,m\Delta t} = y \\ 0 & q_{\alpha,m\Delta t} < y \end{cases} \tag{3}$$

where k denotes nucleation time $\tau=k\Delta\tau$. $\Delta\tau$ and Δt are set to be numerically identical. η_α is the ratio between disc radius and half-thickness. The growth of α_p and α_w is treated similarly as α but with different nucleation rates [6]. Besides, the growth of α_w is modelled as the lengthening of tetragonals instead of discs.

The growth kinetic function of α_b is expressed as [9]:

$$\frac{\mathrm{d}\xi}{\mathrm{d}t} = \frac{uK_1}{X_{\alpha_b,\max}} (1-\xi)\left[1+\lambda_1 (1-\lambda_2 x_\gamma)\, X_{\alpha_b,\max}\xi\right] \times \exp\left[-\frac{K_2}{RT}\left(1+\frac{\Delta F'_{\max}}{C_e}\right) + \frac{K_2}{C_e RT}\left(\Delta F'_{\max} - \Delta F'_N\right)\right] \tag{4}$$

where ξ is the ratio between volume fraction X_{α_b} of current α_b and its maximum value $X_{\alpha_b,\max}$, namely $\xi = X_{\alpha_b} / X_{\alpha_b,\max}$. u is the volume of a bainitic subunit. x_γ is the carbon concentration in steel. C_e, K_1, K_2, λ_1 and λ_2 are fitted constants. R is the gas constant. $\Delta F_{\max}$ is the maximum molar energy difference between γ and α_b. ΔF_N is the energy required for the nucleation of α_b. For α', its final volume faction is estimated as [8]:

$$-\frac{\ln(1-X_{\alpha'})}{X_{\alpha'}} = 1 + C_f (M_s - T) \tag{5}$$

where $X_{\alpha'}$ is the volume fraction of α' at temperature T and C_f is also a fitted constant.

EXPERIMENTAL SETUP

The bead-on-plate specimens of low-alloyed sheet metal S700 were produced using the GMAW, with a thickness of 8.0 mm and a length of 800 mm. The chemical compositions

of plate and filler are listed in Table 1. The welding speed is controlled at 300 mm/min and the other welding conditions are detailed in Table 2, in which 'HI' means heat input.

Table 1 Chemical composition of S700 plate and filler

	Chemical elements (wt.%)			
	C	Si	Mn	Ni + Mo + Cr
Plate	0.06	0.05	1.90	0.70
Filler	0.10	0.90	1.50	

Table 2 The currents and voltages used at three heat input level

Sample	Current (A)	Voltage (V)
Low HI	180	20
Medium HI	210	22
High HI	240	25

As mentioned, BM and filler are mixed in the FZ and the chemical composition is predicted by SimWeld. The uniform values are listed in Table 3.

Table 3 The chemical composition in FZ predicted by SimWeld

	Chemical elements (wt.%)			
	C	Si	Mn	Ni + Mo + Cr
Low HI	0.077	0.47	1.66	0.27
Medium HI	0.077	0.48	1.66	0.26
High HI	0.078	0.49	1.65	0.26

MODEL ESTABLISHMENT

The coupled thermo-metallo-mechanical model incorporates three aspects. In the thermal analysis, the temperature is regenerated in ABAQUS by implementing the double ellipsoidal heat source as:

$$q(x,y,z,t) = \frac{6\sqrt{3} f_f Q_{\text{inp}}}{a_f bc\pi\sqrt{\pi}} \exp\left(-\frac{3\left[x+v(\tau-t)\right]^2}{a_f^2} - \frac{3y^2}{b^2} - \frac{3z^2}{c^2} \right) \tag{6}$$

with the parameters which were calibrated by SimWeld and are summarized in Table 4.

Table 4 The calibrated parameters of double ellipsoidal model by SimWeld

	a_f (mm)	a_r (mm)	b (mm)	c (mm)	f_f	Q_{inp} (W)
Low HI	3.5	14.3	3.7	5.1	1.3	3400
Medium HI	4.0	18.0	4.3	6.0	1.2	4400
High HI	7.0	19.5	4.8	3.2	1.5	5400

f_f is the power fraction of the front ellipsoid. a_f, b and c are the ellipsoid semi-axes. The distribution function in the rear quadrant has the same form but with different values for the semi-axis length a_r and the power fraction f_r. f_f and f_r satisfy $f_f + f_r = 2.0$ [12]. The description and the function of power distribution is shown in Figure 2. The function is implemented in ABAQUS writing user subroutine DFLUX.

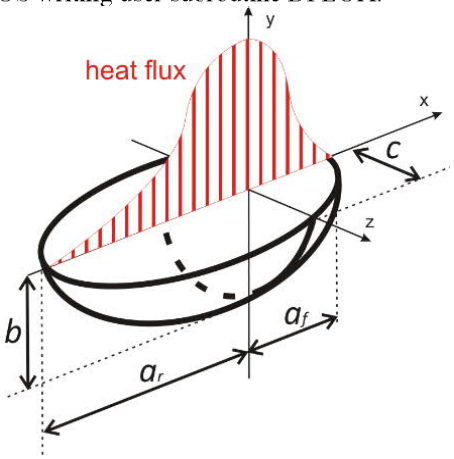

Fig. 2 The power distribution function of double ellipsoidal heat source

As mentioned, the geometry after welding is also predicted by SimWeld. The results are output as '.igs' files and the 2D figures are presented in Figure 3. Those files are imported to ABAQUS to create 3D models.

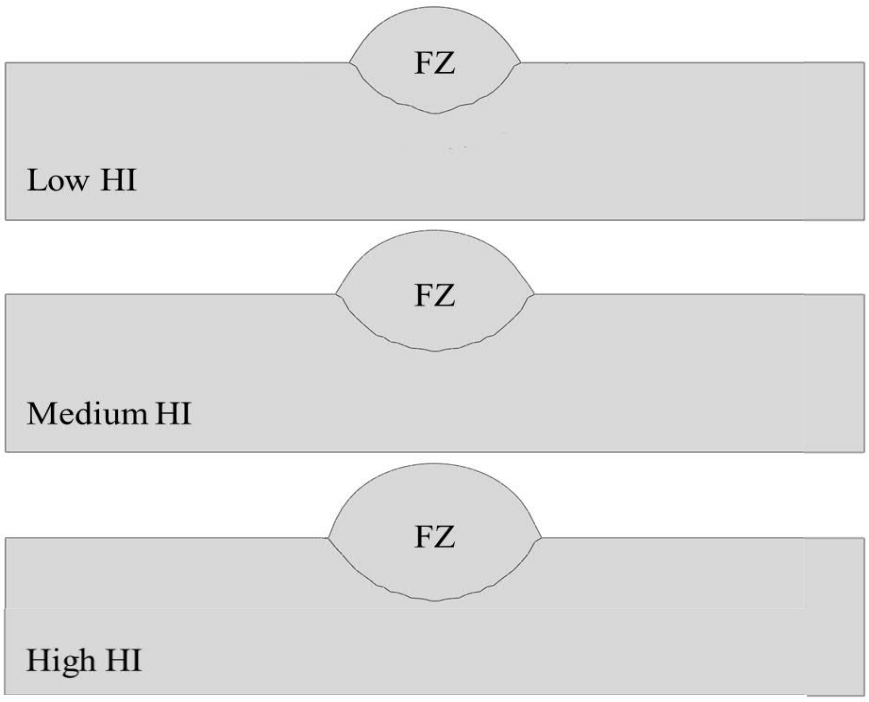

Fig. 3 The geometry of the weld at three heat input levels

The uniform field simply uses the chemical composition of BM for every node. The non-uniform chemistry field is created by the following steps:

- Create the FE model in ABAQUS, and group the nodes belonging to FZ and BM in separate sets. The model is exported as '.inp' file.
- A python script is written to select the nodes belonging to each set and rearrange them in nodal sequence as illustrated in Figure 4 b).
- In the last step, the chemical compositions of FZ (denoted as 'CFUSION' in Figure 4 c)) and BM (denoted as 'CBASE' in Figure 4 c)) are assigned to corresponding nodes.

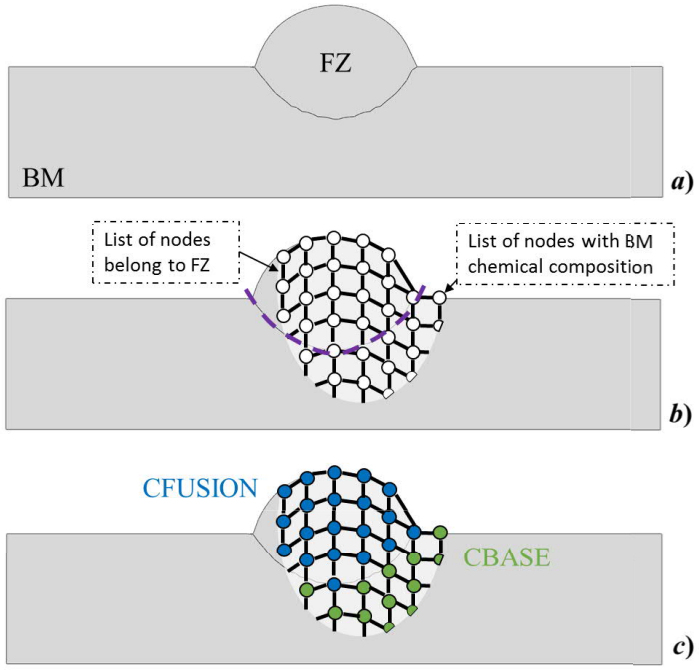

Fig. 4 The steps to construct a chemistry field for simulation

The chemistry distribution created in this 2D geometry is output as a '.dat' file in nodal sequence. The inhomogeneity in the third direction is ignored. The homogeneous chemistry distribution in the FZ is stored in a '.dat' file as well.

The metallurgical algorithm in section 2 is implemented in ABAQUS using another subroutine ABAMAIN. In the algorithm, the start and finish transformation temperatures are estimated based on thermodynamic theories rather than empirical functions. For transforming kinetics, the model assumes the reconstructive transformation to occur at grain boundaries but also includes the possibility of inclusion nucleation. The nucleation rates were treated as temperature-dependent and the growth rates were determined by solving carbon diffusion equations [6]. The initiation of bainite growth was assumed to be displacive with a strain energy of 400 J/mol [13]. The advantages of this framework are that:

- it omits the troubles of parameter validation;
- it requires only the chemical composition, the temperature history and the austenite grain size at each node as its input.

The BM mainly consists of bainite. The SEM micrograph shows that bainite accounts for 99% and that ferrite contributes to 1% [14]. Therefore, the initial values of bainite and ferrite in the metallurgical analysis are assigned to be 0.01 and 0.99 in the FE model. The

values of the other phases are set to 0.00. Again, the five products, allotriomorphic ferrite (α), Widmannstätten ferrite (α_w), pearlite (α_p), bainite (α_b) and martensite (α') are arranged in sequence as in Table 5.

Table 5 The sequence of field variables and corresponding phase stored in ABAQUS

FV1	FV2	FV3	FV4	FV5	FV6
α	α_w	α_p	α_b	α'	γ

The mechanical analysis is conducted using the built-in elasto-plastic algorithm in ABAQUS. The material is treated as an assembly of phases or constituents. Therefore, the overall properties are obtained by linearly interpolating the properties of individual phases with their respective volume fractions.

The mechanical properties are listed in Table 6. The values of α_w are not listed in Table 6 because it is treated the same as α and α_p. The tangent modulus of all phases is assumed to be 2000 MPa [15].

Table 6 The properties of individual phase [16]

		Temperature (°C)			
Property	**Phase**	**0**	**300**	**600**	**800**
Elastic modulus, GPa	γ	200	175	150	124
	α and α_p	210	193	165	120
	α_b	210	193	165	120
	α'	200	185	168	--
Poisson's ratio	γ	0.29	0.31	0.33	0.35
	α and α_p	0.28	0.30	0.31	0.33
	α_b	0.28	0.30	0.31	0.33
	α'	0.28	0.30	0.31	--
Expansion coefficient, K^{-1}	γ	2.1×10^{-5}			
	α and α_p	1.4×10^{-5}			
	α_b	1.4×10^{-5}			
	α'	1.3×10^{-5}			
Yield strength, MPa	γ	190	110	30	20
	α and α_p	360	230	140	30
	α_b	440	330	140	30
	α'	1600	1480	1260	--

The implementation algorithm is plotted in Figure 5. One thermal analysis is run before the coupled analysis to produce the temperature field. Therefore, the proposed model is sequentially coupled, ignoring the effects of latent heat and plastic work. This is reasonable since the amount of energy produced by those mechanisms is far lower than the input heat power [17, 18]. The experiments were conducted at a room temperature of 20°C, with an estimated convection coefficient of $30 W/m^2°C$.

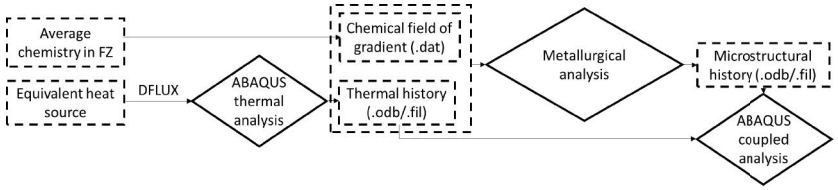

Fig. 5 Flow chart of the fully coupled model

RESULTS AND DISCUSSION

The microstructure evolution of two selected nodes, 'A' and 'B', predicted in high heat input are plotted in Figure 6. Here, only the distribution of α and α_w are presented because they are the main transformation products. The evolution line of the homogeneously distributed chemistry field is drawn in black, comparing to the results of the inhomogeneous chemistry distribution in red. The nodes are chosen at the middle cross-section of the weld. 'A' is located at the top of the section. 'B' lies at the FZ/HAZ boundary. The difference of α and α_w volume fractions at node 'A' can be obviously noticed. It is due to the fact that point 'A' in inhomogeneous model possesses a chemical composition different from BM as presented in Table 3. Moreover, higher volume fraction of α at 'A' is found in the case of inhomogeneous chemistry, while the value of α_w is lower. This phenomenon indicates that the chemistry of the filler wire favors the formation of α and inhibits the production of α_w. For location 'B', the microstructure evolutions predicted by both chemistry fields are identical according to the algorithm in section 4. As a result, their volume fractions overlap with each other.

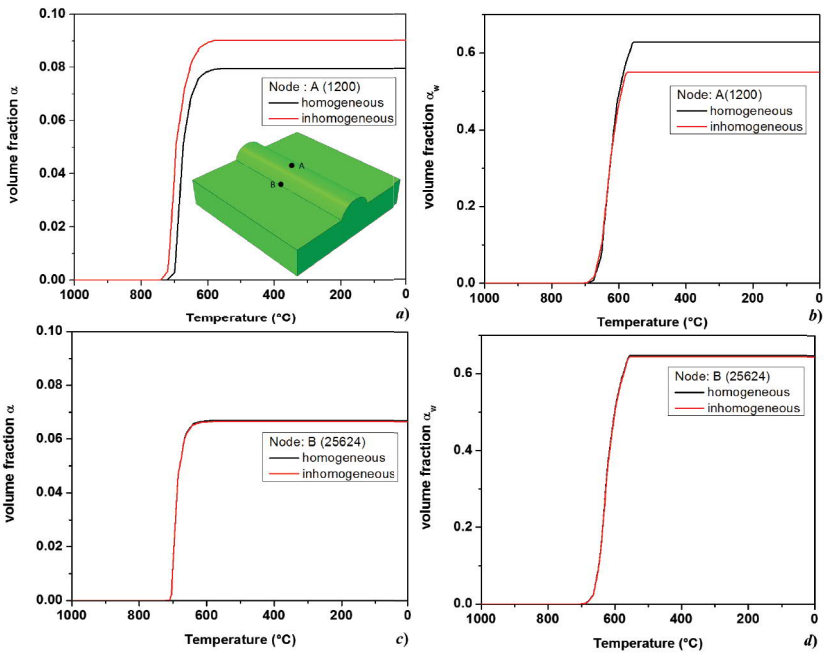

Fig. 6 The evolution of α and α_w at specific positions 'A' and 'B'

Previously, the microstructure evolution was plotted only for the high level heat input. To demonstrate the effect of chemistry inhomogeneity at different heat input levels, the final distributions of α' in all cases are presented in Figure 7. With the decrease of input power, the cooling rate increases in the FZ and the volume fraction of α' increases accordingly. However, due to the reduction of heat input, the transformation occurs within a smaller area. The maximum value of α' predicted by the inhomogeneous field is always greater than the one by the homogeneous field. This is caused by the fact that in the inhomogeneous field, the carbon concentration is higher than the one in the uniform field. The distributions of α' volume fraction are different either, especially in FZ, which is again caused by the chemistry inhomogeneity. However, this distribution difference becomes not so significant in the low heat input level, which may be due to the fact that the cooling rate turns out to be the main fact influencing on the phase transformation.

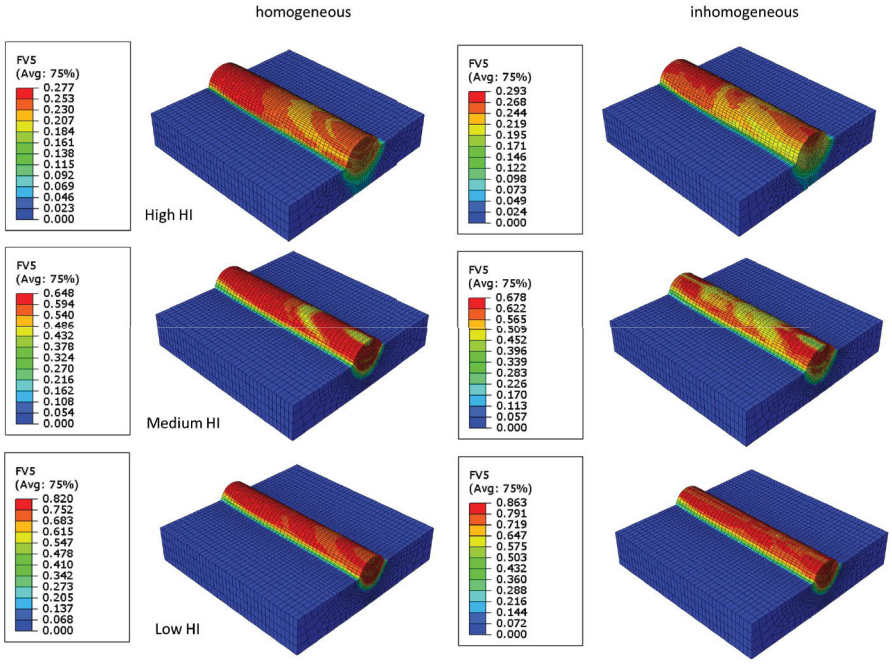

Fig. 7 The contour plots of α' predicted using homogeneous and inhomogeneous fields

Finally, the stress distributions at the middle cross-section are plotted in Figure 8. 'S11' is the stress component vertical to the section, and 'S33' is the parallel value. The maximum stress values predicted using the inhomogeneous field, no matter in tensile or compressive, stay lower than the values of the homogeneous one. Furthermore, compared to the distribution of 'S11' of the homogeneous field, the area subjected to tensile stress predicted by the inhomogeneous field expands. Similar situation is found for the 'S33' distribution.

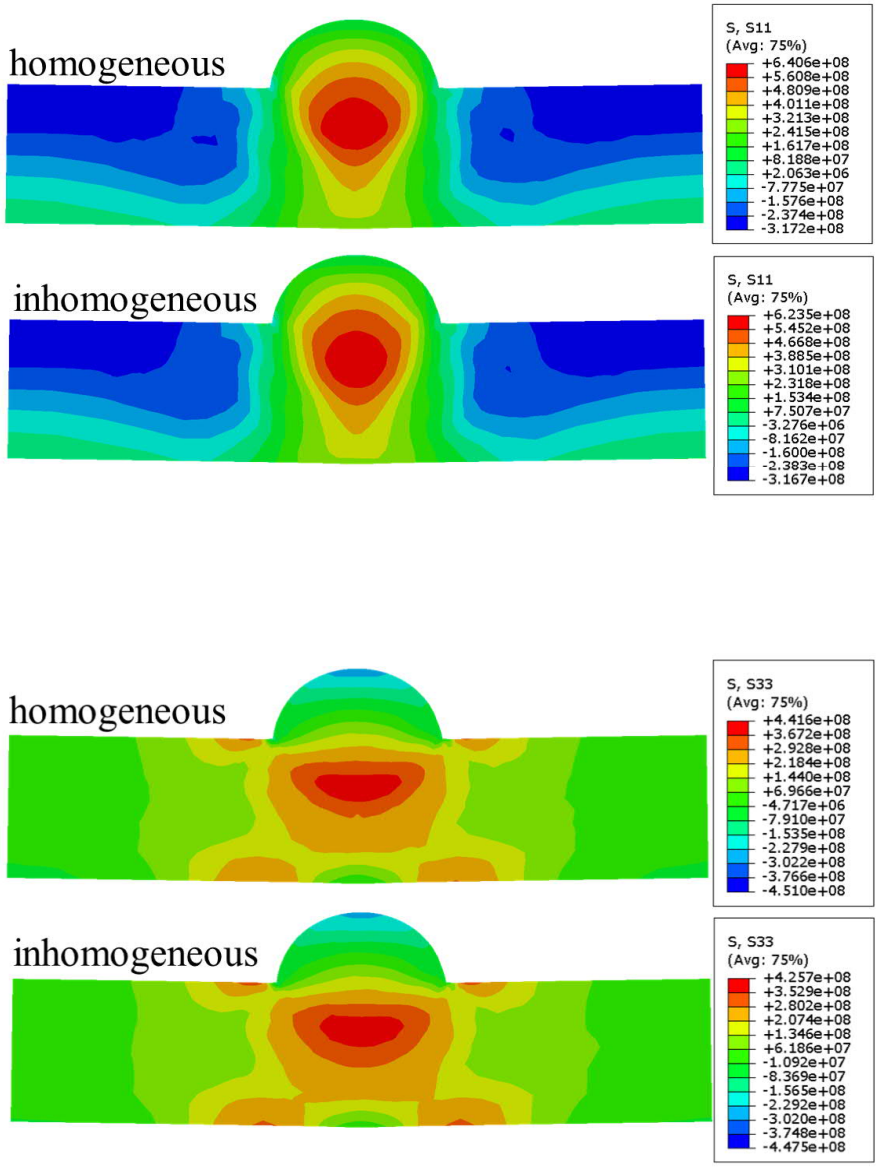

Fig. 8 The stress distribution at the middle cross-section

CONCLUSION

A metallurgical algorithm by Bhadeshia et al. [6-9] is implemented in ABAQUS to establish a coupled thermo-metallo-mechanical model. To analyze the effects of chemical composition on the phase transformation and the residual stress, the chemical composition predicted by SimWeld is adopted to construct a reasonable inhomogeneous chemistry field. This field is further imported to the coupled FE analysis. By comparing the simulation results using homogeneous and inhomogeneous fields, the following conclusions can be drawn:

- At high heat input level, more α and less α_w are produced in FZ due to the chemistry inhomogeneity, while at the FZ/HAZ boundary, no difference of the volume fractions of α and α_w is found.
- Higher heat input reduces α' volume fraction.
- The non-uniform chemistry increases the maximum value as well as the distribution of α' volume fraction in the simulation results.
- The inhomogeneous chemistry distribution reduces the maximum magnitudes of the residual stress components and extends the areas subjected to tensile stress.

ACKNOWLEDGEMENTS

The authors acknowledge the MaDurOS project and the support from SIM and VLAIO.

REFERENCES

[1] H. K. D. H. BHADESHIA: 'A Rationalization of Shear Transformations in Steels', *Acta Metallurgica*, Vol. 29, No. 6, pp. 1117-1130, 1981.

[2] A. A. BHATTI, Z. BARSOUM, H. MURAKAWA, and I. BARSOUM: 'Influence of Thermo-Mechanical Material Properties of Different Steel Grades on Welding Residual Stresses and Angular Distortion', *Materials & Design*, Vol. 65, pp. 878-889, 2015.

[3] L. BORJESSON, AND L. E. LINDGREN: 'Simulation of Multipass Welding with Simultaneous Computation of Material Properties', *Journal of Engineering Materials and Technology-Transactions of the ASME*, Vol. 123, No. 1, pp. 106-111, 2001.

[4] A. A. BUKI: 'Calculating the Chemical Composition of Deposited Metal When Welding with Coated Electrodes', *Welding International*, Vol. 6, No. 10, pp. 818-820, 1992.

[5] HUI DAI: 'Modelling Residual Stress and Phase Transformations in Steel Welds', *INTECH Open Access Publisher*, 2012.

[6] D. DENG: 'FEM Prediction of Welding Residual Stress and Distortion in Carbon Steel Considering Phase Transformation Effects', *Materials & Design*, Vol. 30, No. 2, pp.359 -366, 2009.

[7] P. FERRO, H. PORZNER, A. TIZIANI, AND F. BONOLLO: 'The Influence of Phase Transformations on Residual Stresses Induced by the Welding Process - 3d and 2d Numerical Models', *Modelling and Simulation in Materials Science and Engineering*, Vol. 14, No. 2, pp.117 -136, 2006.

[8] JOHN A GOLDAK, AND MEHDI AKHLAGHI: *Computational Welding Mechanics*, Springer Science & Business Media, 2006.

[9] W. GUO, J. A. FRANCIS, L. LI, A. N. VASILEIOU, D. CROWTHER, AND A. THOMPSON: 'Residual Stress Distributions in Laser and Gas-Metal-Arc Welded High-Strength Steel Plates', *Materials Science and Technology*, Vol. 32, No. 14, pp. 1449-1461, 2016.

[10] C. J. HAMELIN, O. MURANSKY, M. C. SMITH, T. M. HOLDEN, V. LUZIN, P. J. BENDEICH, AND L. EDWARDS: 'Validation of a Numerical Model Used to Predict Phase Distribution and Residual Stress in Ferritic Steel Weldments', *Acta Materialia*, Vol. 75, pp.1-19, 2014.

[11] S. J. JONES, AND H. K. D. H. BHADESHIA: 'Kinetics of the Simultaneous Decomposition of Austenite into Several Transformation Products', *Acta Materialia*, Vol. 45, No. 7, pp.2911-2920, 1997.

[12] S. A. KHAN, AND H. K. D. H. BHADESHIA: 'Kinetics of Martensitic-Transformation in Partially Bainitic 300m Steel', *Materials Science and Engineering AStructural Materials Properties Microstructure and Processing*, Vol. 129, No. 2, pp. 257-272, 1990.

[13] J. S. KIRKALDY, AND R. C. SHARMA: 'A New Phenomenology for Steel It and Cct Curves', *Scripta Metallurgica*, Vol. 16, No. 10, pp. 1193-1198, 1982.

[14] R. C. REED, AND H. K. D. H. BHADESHIA: 'Kinetics of Reconstructive Austenite to Ferrite Transformation in Low-Alloy Steels', *Materials Science and Technology*, Vol. 8, No. 5, pp. 421-435, 1992.

[15] G. I. REES, AND H. K. D. H. BHADESHIA: 'Bainite Transformation Kinetics .1. Modified-Model', *Materials Science and Technology*, Vol. 8, No. 11, pp. 985-993, 1992.

[16] F.N. RHINES, R.T. DEHOFF: *Quantitative Microscopy*, University of Florida, 1968.

[17] M. TAKAHASHI, AND H. K. D. H. BHADESHIA: 'A Model for the Microstructure of Some Advanced Bainitic Steels', *Materials Transactions*, Vol. 32, No. 8, pp. 689-696, 1991.

[18] G.E. TOTTEN: *Handbook of Residual Stress and Deformation of Steel*, ASM International, 2002.